Influence of phase connectivity on the relationship among capillary pressure, fluid saturation, and interfacial area in two-fluid-phase porous medium systems

James E. McClure, Mark A. Berrill, William G. Gray, and Cass T. Miller

Phys. Rev. E **94**, 033102 — Published 2 September 2016

DOI: 10.1103/PhysRevE.94.033102

ailmcclurej@vt.edu

Influence of Phase Connectivity on the Relationship Among Capillary Pressure, Fluid Saturation, and Interfacial Area in Two-Fluid-Phase Porous Medium Systems

James E. McClure
Advanced Research Computing, Virginia Tech, Blacksburg, Virginia 24061-0123

Mark A. Berrill*
Oak Ridge National Laboratory, Tennessee, USA

William G. Gray and Cass T. Miller
Department of Environmental Sciences and Engineering
University of North Carolina, Chapel Hill, North Carolina 27599
(Dated: August 2, 2016)

Multiphase flows in porous medium systems are typically modeled at the macroscale by applying the principles of continuum mechanics to develop models that describe the behavior of averaged quantities, such as fluid pressure and saturation. These models require closure relations to produce solvable forms. One of these required closure relations is an expression relating the capillary pressure to fluid saturation and, in some cases, other topological invariants such as interfacial area and the Euler characteristic (or average Gaussian curvature). The forms that are used in traditional models, which typically consider only the relationship between capillary pressure and saturation, are hysteretic. An unresolved question is whether the inclusion of additional morphological and topological measures can lead to a non-hysteretic closure relation. Relying on the lattice Boltzmann (LB) method, we develop an approach to investigate equilibrium states for a two-fluid-phase porous medium system, which includes disconnected non-wetting phase features. A set of simulations are performed within a random close pack of 1,964 spheres to produce a total of 42,908 distinct equilibrium configurations. This information is evaluated using generalized additive models to quantitatively assess the degree to which functional relationships can explain the behavior of the equilibrium data. The variance of various model estimates is computed, and we conclude that, except for the limiting behavior close to a single fluid regime, capillary pressure can be expressed as a deterministic and non-hysteretic function of fluid saturation, interfacial area between the fluid phases, and the Euler characteristic. This work is unique in the methods employed, the size of the data set, the resolution in space and time, the true equilibrium nature of the data, the parameterizations investigated, and the broad set of functions examined. The conclusion of essentially non-hysteretic behavior provides support for an evolving class of two-fluid-phase flow in porous medium systems models.

I. INTRODUCTION

Multiphase systems arise routinely in subsurface environments. Examples include geologic carbon sequestration [1–3], vadose zone hydrology, and oil and gas recovery [4]. Engineered systems such as fuel cells are also multiphase porous medium systems [5–8]. The challenges associated with multiphase flow through porous media are widely recognized, and sustained efforts have been made to better understand the physics of these flow processes [9–16]. Mathematical models that describe transport phenomena in these systems are routinely used to test understanding, predict future states, and support design and management decisions. Models must capture essential multiscale physics that determine system behavior. Because natural porous medium systems must often be described at length scales that are long compared to the natural length scale, which corresponds to a grain diameter or a characteristic length or aperture of a fracture, macroscale models are commonly used. Macroscale models are posed in terms of averaged properties over a length scale that yields an averaging domain containing representative extents of all of the entities (phases, interfaces, and common curves). Physical processes that occur at small length scales must be represented adequately within the macroscale description. Multiscale theories and models that formalize the connection between the microscale and the macroscale can be used to methodically advance understanding, and are of funda-

mental importance within this context.

Fundamental study of transport phenomena in porous medium systems is often undertaken at the microscale, where the morphology and topology of the phase distributions are resolved in space and in time. The physics of multiphase transport phenomena are relatively well understood at the microscale as compared to the macroscale. Methodologies designed to directly access microscale information as a way to advance macroscale understanding have become widespread [17–25]. Such studies have yielded many enhancements to our understanding of pore-scale transport mechanisms involved in multiphase flow [26–29]. Unfortunately, macroscale models are often posed directly at the macroscale and lack a rigorous connection to the microscale. Consequently, quantities that are known to be important at the microscale (such as contact angles, interfacial tensions, curvatures, and areas, and common curve properties) do not appear explicitly in common macroscale model formulations. Closure relations relating fluid pressures to fluid saturations are required, but depend on the physical processes that lead to a particular system state. This so-called hysteresis has been posited to result from an implicit representation of the underlying microscale physics in empirical model forms and coefficients used to close macroscale equations [30]. Efforts to describe capillary pressure within macroscale models is an active research area [e.g. 31, 32].

The thermodynamically constrained averaging theory (TCAT) provides a systematic approach to construct mathematical models of multiscale transport phenomena in which thermodynamics are used to constrain the allowable form of closure relations. The TCAT approach has been applied to produce macroscale models for several types of porous medium systems [30]. A major contribution of the method is that a consistent upscaling procedure is applied such that all macroscopic variables are concretely defined in terms of averaged forms of microscale quantities. This is significant because the precursor conservation equations and thermodynamics are well-understood at the microscale, from the standpoint of continuum mechanics, classical thermodynamics, and kinetic theory. Macroscopic definitions of thermodynamic quantities such as pressure, temperature, and entropy are derived precisely from microscale quantities to ensure that the macroscopic models that are produced observe the laws of thermodynamics [30]. Similarly, the conditions that must apply at equilibrium at the macroscale for multiphase systems have also been derived using variational methods and rigorous upscaling from the microscale. TCAT naturally incorporates essential components from thermodynamics, conservation principles, and fundamental geometric relationships.

To describe the thermodynamics of a multiphase system, it is necessary to account for the thermodynamics of phases, the interfaces where two phases meet, and the common curve where all three phases are present. This is true because the total energy of the system includes contributions from each of these entities (phases, interfaces, and common curves). Interfacial areas are important extensive properties of a multiphase system that are associated with a non-negligible fraction of the system energy at equilibrium. Traditionally, these energy contributions have been ignored in macroscopic models of multiphase porous medium systems. More recently, interfacial areas have been posited to be an important state variable needed to describe fluid states in a two-fluid-phase porous medium system that must be accounted for to reduce or eliminate hysteresis observed in the macroscale relationship between capillary pressure and fluid saturation [33]. Technologies such as micro-computed tomography (μCT) have made it possible to observe directly the three-dimensional microstructure of real porous media, including the interfacial configurations [34–42]. Numerical simulation tools can also provide this information [43–47]. As information about the interfacial behavior has become more accessible, many authors have undertaken experimental and numerical efforts to incorporate interfacial areas into closure relations for multiphase porous medium systems [e.g. 30, 48–50]. A large number of equilibrium states must be considered to assess whether or not these relationships are truly unique, and careful theoretical analysis is required to deduce a representation of the relationship among state variables.

The presence of disconnected non-wetting phases has received sustained study, including investigations focused on the statistical distribution of disconnected phases and their role in macroscopic equilibrium relationships [51–57]. Entrapped non-wetting phases are routinely present in multiphase porous medium systems, with important ramifications for both the equilibrium state and transport phenomena [51, 58]. Regions of non-wetting phase become trapped, and disconnected, with a particular capillary pressure; pressure gradients will not be transmitted between different disconnected regions of the non-wetting phase. Accounting for disconnected phase regions is essential to properly account for both the equilibrium state and dynamic behavior of multiphase systems [47, 59, 60]. Efforts to adequately account for the connectivity and topology of the multiphase fluid configurations is therefore of great potential importance to develop a more comprehensive understanding of these complex transport processes [42, 61].

In a general sense, a macroscopic equilibrium relationship must account for the possible microscale equilibrium states of a system and describe the internal energy that results from those states. In subsurface porous medium systems, many different physical processes can influence the microscale state. Examples include changes in temperature or pressure, phase changes, chemical reactions and mechanical stimulation from acoustic or seismic activity. It is essential to consider all possible microscale states that may arise as a consequence of these processes if one wishes to develop a general macroscale closure relation.

Exploration of the range of possible equilibrium states

is not possible from standard experimental setups in which fluid distributions are controlled through manipulation of boundary conditions of the system alone. In standard experiments, fluid saturations and pressures are measured based upon boundary conditions, yet fluid pressures measured at the boundary of a system do not account for the pressures of any fluids that are not connected to that boundary. Examples of processes affecting fluid configurations that are inaccessible from standard experiments are evaporation and transpiration, which can lead to wetting phase saturations that are lower than the so-called "irreducible saturation" frequently observed in traditional experimental setups [62–66]. These states occur routinely, suggesting that alternative approaches should be developed to better account for a more complete range of equilibrium states [67].

It has also been observed that changes in wettability can occur dynamically within multiphase porous medium systems [68, 69]. Dissolution of an entrapped non-wetting phase is a key mechanism to sequester carbon dioxide in the subsurface. As individual features dissolve, their size decreases and the resulting equilibrium state must also change. Such processes invariably lead to multiphase fluid configurations that are not observed during traditional drainage and imbibition experiments based on established experimental procedures. Nevertheless, a complete thermodynamic description of a multiphase system must be capable of describing the state of a system irrespective of the system history. To be fully general, one must consider all possible microscale states; it is not sufficient to consider only a subset of these states, such as those that arise from a particular flow process or experimental design.

The overall goal of this work is to characterize the equilibrium behavior of two-fluid-phase porous medium systems. The specific objectives of this work are as follows:

1. to develop a theoretical framework to analyze microscale states in the context of phase connectivity;
2. to advance an efficient computational approach to generate independent realizations of possible microscale states in multiphase porous medium systems;
3. to evaluate the macroscale states that correspond to the generated microscale equilibrium states; and
4. to evaluate the uniqueness of various parameterizations of capillary pressure.

II. THEORY

We consider averages for a two-fluid-phase porous medium system within a domain Ω with boundary Γ. Three phases are present, denoted with a corresponding index for the wetting phase (w) the non-wetting phase (n) and the solid (s). Each of the phases occupies a three-dimensional subset of Ω, denoted by Ω_w, Ω_n and Ω_s, respectively. The corresponding closed domains, which include the boundaries, are $\bar{\Omega}_w = \Omega_w \cup \Gamma_w$, $\bar{\Omega}_n = \Omega_n \cup \Gamma_n$, and $\bar{\Omega}_s = \Omega_s \cup \Gamma_s$. Since three phases are present, three interface types are possible, each of which occupies a two-dimensional subdomain within Ω. These include the interface between the wetting and non-wetting fluids, denoted by Ω_{wn}, the interface between the wetting fluid and the solid, Ω_{ws}, and the interface between the non-wetting fluid and the solid, Ω_{ns}. Finally, a common curve can exist where all three phases meet, which is a one-dimensional subdomain within Ω denoted by Ω_{wns}. The complete set of entities for the two-fluid phase system includes all phases and interfaces in addition to the common curve, which together comprise the index set of entities, $\mathcal{I} = \{w, n, s, wn, ws, ns, wns\} = \mathcal{I}_\mathrm{P} \cup \mathcal{I}_\mathrm{I} \cup \mathcal{I}_\mathrm{C}$, where $\mathcal{I}_\mathrm{P}$ is the index set of phases, $\mathcal{I}_\mathrm{I}$ is the index set of interfaces, and $\mathcal{I}_\mathrm{C}$ is the index set of common curves. It will also be convenient to refer to $\mathcal{I}_\mathrm{f}$, which is the index set of fluid phases expressed as $\mathcal{I}_\mathrm{f} = \{w, n\}$. The corresponding domain occupied by the fluid phases is denoted by Ω_f. For the interfaces and common curve the order of phase indexes comprising an entity index is not important. For example, Ω_{wn} and Ω_{nw} both refer to the same wetting phase-non-wetting phase interfacial domain.

Macroscale TCAT models involve the systematic upscaling of microscale thermodynamic relations as well as conservation and balance equations to the macroscale using averaging operators and theorems [30]. An element of this procedure is the upscaling to the macroscale of microscale thermodynamic equilibrium conditions, which can be derived using variational methods. Of special interest are macroscale state equations that are needed for a closed model and which express a posited functional from among macroscale variables. Meeting the objectives of this work requires an examination of certain averaged quantities arising from upscaling from the microscale to the macroscale.

The macroscale averages of concern herein are computed using an averaging operator of the form

$$\langle P \rangle_{\Omega_\alpha, \Omega_\beta} = \frac{\int_{\Omega_\alpha} P \, \mathrm{d}\mathfrak{r}}{\int_{\Omega_\beta} \mathrm{d}\mathfrak{r}} \, , \tag{1}$$

where P is a microscale property and Ω_α and Ω_β are domains of integration. Averages of interest include extent measures for each entity in the system, such as fluid volume fractions, specific interfacial areas, and the specific common curve length. These extent measures are computed as

$$\epsilon^{\overline{\overline{\alpha}}} = \langle 1 \rangle_{\Omega_\alpha, \Omega} \quad \text{for } \alpha \in \mathcal{I} \, , \tag{2}$$

where the double-barred superscript denotes a specially defined macroscale variable. Eq. (2) defines a volume fraction when $\alpha \in \mathcal{I}_\mathrm{P}$, a specific interfacial area when $\alpha \in \mathcal{I}_\mathrm{I}$, and a specific common curve length when $\alpha = \mathcal{I}_\mathrm{C}$. The fluid saturations are determined as

$$s^{\overline{\overline{\alpha}}} = \langle 1 \rangle_{\Omega_\alpha, \Omega_f} \quad \text{for } \alpha \in \mathcal{I}_\mathrm{f} \, . \tag{3}$$

The intrinsic macroscale averaged fluid-phase pressures are computed as intrinsic volume averages over the respective phases as

$$p^{\alpha} = \langle p_{\alpha} \rangle_{\Omega_{\alpha},\Omega_{\alpha}} \quad \text{for } \alpha \in \mathfrak{I}_{\mathrm{f}} \ , \tag{4}$$

where p_{α} is the microscale fluid pressure.

The nature of the equation of state relating capillary pressure, fluid saturations, and specific interfacial areas is of essential importance. The macroscale capillary pressure between the wetting and non-wetting fluid phases is defined as

$$p^{wn} = -\langle \gamma_{wn} J_w \rangle_{\Omega_{wn},\Omega_{wn}} = \langle p_{wn} \rangle_{\Omega_{wn},\Omega_{wn}} \ , \tag{5}$$

where γ_{wn} is the microscale interfacial tension between the two fluid phases, $J_w = \nabla' \cdot \mathbf{n}_w$ is the mean microscale curvature of the interface, and $\mathbf{n}_w$ is the outward unit normal vector from the w phase. The negative sign accounts for the convention that capillary pressure is a non-negative quantity, and the curvature of the interface between the wetting and non-wetting fluids is measured by the surface divergence of the outward normal vector from the wetting phase.

The Euler characteristic is an invariant topological measure that is linked to the connectivity of an object. Along with the volume, surface area, and integral of mean curvature, the Euler characteristic is one of four invariant topological measures that is used to characterize three-dimensional objects based on integral geometry [70–72]. The results of integral geometry have been applied broadly to characterize the microstructure of porous materials [73–77]. The Euler characteristic χ is most often computed by counting the number of vertices V, edges E, and faces F on the surface of a closed object

$$\chi = V - E + F \ . \tag{6}$$

Equivalent definitions for χ are well-known within the field of topology. The Euler characteristic can also be computed from the Betti numbers, which relate the definition of χ to the connectivity of an object. For a three-dimensional object, the Euler characteristic can be written as

$$\chi = B_0 - B_1 + B_2 \ . \tag{7}$$

Each of the Betti numbers has a physical interpretation: B_0 is the number of connected components; B_1 is the number of redundant pathways (or tunnels); and B_2 is the number of cavities [78]. This interpretation ties the Euler characteristic of an object to invariant aspects of the connectivity of that object. For a fluid phase, connectivity will clearly influence transport within the phase since this aspect of topology determines the flow paths and energetic states that are accessible.

A third theoretical result relates the Euler characteristic of an object to the integral curvature over the boundary of that object. This definition allows the Euler characteristic of a phase to be expressed as an average in the general form of Eq. (1). Based on the Gauss-Bonnet theorem, the normalized Euler characteristic per unit volume of the domain relates to the average of the Gaussian curvature K_{α} over the closed phase boundary Γ_{α}

$$\chi^{\overline{\overline{\alpha}}} = \frac{1}{2\pi} \langle K_{\alpha} \rangle_{\Gamma_{\alpha},\Omega} \ . \tag{8}$$

In practice, an approximation to $\chi^{\overline{\overline{\alpha}}}$ can be obtained by constructing a numerical approximation to $\bar{\Omega}_{\alpha}$ using the marching cubes algorithm and counting the vertices, faces and edges [79]. The computed Euler characteristic is then normalized by dividing by the total volume of the domain.

In two-fluid-phase porous medium systems, the fluid phases can become disconnected because of the interplay among capillary, viscous, and gravitational forces, which can lead to mechanisms such as non-wetting phase snap off and unstable displacement patterns. To account for these well-known physical phenomena, we consider the implications of such fluid distributions on macroscale variables and thermodynamic equilibrium conditions. To do this, we decompose the domain for a fluid phase Ω_{α} into connected regions. The connected regions are a set of subdomains Ω_{α_j} where $j \in \mathcal{N}_{\alpha} = \{1, 2, \ldots, N_{\alpha}\}$, where N_{α} is the total number of connected components for the α fluid phase. The subdomains satisfy the equations

$$\Omega_{\alpha_i} \cap \Omega_{\alpha_j} = \emptyset \quad \forall i, j \in \mathcal{N}_{\alpha} \wedge i \neq j \ , \text{ and} \tag{9}$$

$$\Omega_{\alpha} = \cup_{i=1}^{N_{\alpha}} \Omega_{\alpha_i} \ . \tag{10}$$

That is, the connected subdomain regions Ω_{α_i} do not intersect with other members of the set of connected regions, and the union of the domains of all members of the set of connected regions yield the entire domain of the respective fluid phase. The number of connected regions of a phase is the zeroth Betti number B_0^{α}, which is also the cardinality of the set $\mathcal{N}_{\alpha}$.

An example two-dimensional system illustrating the subdivision of phases within a two-fluid system is shown in Fig. 1. In this case, the wetting phase (blue) can be sub-divided into three connected regions, denoted as $\Omega_{w_1}, \Omega_{w_2}$ and Ω_{w_3}. The intersection between any two of the three wetting-phase regions is the null set, since the boundary of each sub-region touches only non-wetting phase (red) or solid (black). Likewise, the non-wetting phase can be sub-divided into two connected regions, Ω_{n_1} and Ω_{n_2}. Mechanical equilibrium can only be achieved if a balance of forces exists for each interfacial region. Laplace's law relates the curvature of an interface to the pressure difference between two adjoining phases. Based on this, different pressures may be obtained within each connected region, subject to mechanical equilibrium criteria for each region of the interface. For example, the interfacial region identified in yellow and green may have different interfacial curvatures at equilibrium. To describe the equilibria in general, we must sub-divide the interfacial regions based on the underlying phase connectivity.

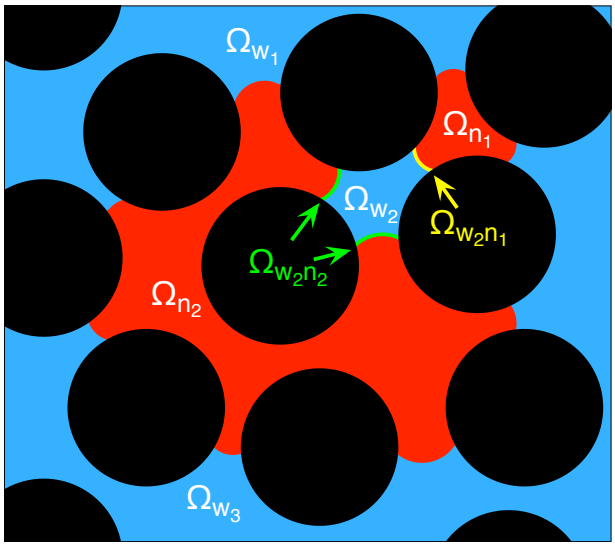

FIG. 1. Phase regions within an example porous medium (black): both the wetting (blue) and non-wetting (red) phases can be sub-divided into connected regions. The interfaces between fluids can also be sub-divided based on connectivity. For example, the fluid interface region labeled in yellow is formed as $\Omega_{w_2 n_1} = \Omega_{w_2} \cap \Omega_{n_1}$, while the region formed in green is formed as $\Omega_{w_2 n_2} = \Omega_{w_2} \cap \Omega_{n_2}$.

Subsets can be determined for the interfacial regions by considering the intersection of the closed domains of two phases such that

$$\Omega_{\alpha_i \beta_j} = \bar{\Omega}_{\alpha_i} \cap \bar{\Omega}_{\beta_j} \quad \text{for } \alpha, \beta \in \mathcal{I}_\text{P}, \alpha \neq \beta \ . \tag{11}$$

The identification of sub-regions of the interface based on the phase connectivity is illustrated in the example system of Fig. 1. Common curve regions associated with the intersection of the closed domains of three phases can be identified as

$$\Omega_{\alpha_i \beta_j \gamma_k} = \bar{\Omega}_{\alpha_i} \cap \bar{\Omega}_{\beta_j} \cap \bar{\Omega}_{\gamma_k} \quad \text{for } \alpha, \beta, \gamma \in \mathcal{I}_\text{P}, \alpha \neq \beta \neq \gamma \ , \tag{12}$$

where i, j, and k are indices for a phase region.

Let the set $\mathcal{N}_\alpha$, for $\alpha \in \mathcal{I}_\text{I}$ contain all pairs of phase region indices that result in a domain with a non-zero extent. For common curves, let $\mathcal{N}_\alpha$ for $\alpha \in \mathcal{I}_\text{C}$ contain all triples of phase region indices that result in a domain with a non-zero extent. The resultant domains account for regions of space occupied by that part of the interface or common curves that are associated with the intersection of the respective phase region domains, respectively. Certain phase regions might not intersect, so some combinations of phase regions will yield a domain with an extent measure of zero.

If an index of a phase qualifier is omitted, then summation is implied. For example, it follows that

$$\Omega_{\alpha_l \beta} = \Omega_{\alpha\beta} \cap \bar{\Omega}_{\alpha_l} = \sum_{\substack{ij \in \mathcal{N}_{\alpha\beta} \\ i=l}} \Omega_{\alpha_i \beta_j} \ , \tag{13}$$

which is the fraction of the total $\Omega_{\alpha\beta}$ interface formed by an intersection with the closed phase region $\bar{\Omega}_{\alpha_l}$. It follows that when both indices are contracted that

$$\Omega_{\alpha\beta} = \sum_{ij \in \mathcal{N}_{\alpha\beta}} \Omega_{\alpha_i \beta_j} \ , \tag{14}$$

which is the total $\alpha\beta$ interfacial domain. Similarly, the fraction of a common curve domain formed by an intersection involving a closed phase region is

$$\Omega_{\alpha_l \beta\gamma} = \Omega_{\alpha\beta\gamma} \cap \bar{\Omega}_{\alpha_l} = \sum_{\substack{ijk \in \mathcal{N}_{\alpha\beta\gamma} \\ i=l}} \Omega_{\alpha_i \beta_j \gamma_k} \ , \tag{15}$$

and the fraction of a common curve domain formed by an intersection involving two closed phase regions, or an interface, is

$$\Omega_{\alpha_l \beta_m \gamma} = \Omega_{\alpha\beta\gamma} \cap \bar{\Omega}_{\alpha_l} \cap \bar{\Omega}_{\beta_m} = \sum_{\substack{ijk \in \mathcal{N}_{\alpha\beta\gamma} \\ i=l, j=m}} \Omega_{\alpha_i \beta_j \gamma_k} \ . \tag{16}$$

It follows that when all indices of a common curve are contracted that

$$\Omega_{\alpha\beta\gamma} = \sum_{ijk \in \mathcal{N}_{\alpha\beta\gamma}} \Omega_{\alpha_i \beta_j \gamma_k} \ , \tag{17}$$

which is the total $\alpha\beta\gamma$ common curve domain. Because all order combinations of an entry in an index set $\mathcal{N}_\alpha, \alpha \in \mathcal{I}_\text{I} \cup \mathcal{I}_\text{C}$ are equivalent, the definitions given by Eqs. (13) – (17) define all fractional domains associated with a specific closed phase region(s).

The averaging operator can also be applied over regions of a domain and summed to yield the overall macroscale averages, which can be written for a phase as

$$\langle P \rangle_{\Omega_\alpha, \Omega_\kappa} = \sum_{i \in \mathcal{N}_\alpha} \langle P \rangle_{\Omega_{\alpha_i}, \Omega_\kappa} \quad \text{for } \alpha \in \mathcal{I}_\text{P} \ , \tag{18}$$

for an $\alpha\beta$ interface as

$$\langle P \rangle_{\Omega_{\alpha\beta}, \Omega_\kappa} = \sum_{i \in \mathcal{N}_\alpha} \langle P \rangle_{\Omega_{\alpha_i \beta}, \Omega_\kappa} \quad \text{for } \alpha, \beta \in \mathcal{I}_\text{P} \ , \tag{19}$$

and for a common curve as

$$\langle P \rangle_{\Omega_{\alpha\beta\gamma}, \Omega_\kappa} = \sum_{i \in \mathcal{N}_\alpha} \langle P \rangle_{\Omega_{\alpha_i, \beta, \gamma}, \Omega_\kappa} \quad \text{for } \alpha, \beta, \gamma \in \mathcal{I}_\text{P} \ , \tag{20}$$

or

$$\langle P \rangle_{\Omega_{\alpha\beta\gamma}, \Omega_\kappa} = \sum_{\substack{i \in \mathcal{N}_\alpha \\ j \in \mathcal{N}_\beta}} \langle P \rangle_{\Omega_{\alpha_i, \beta_j, \gamma}, \Omega_\kappa} \quad \text{for } \alpha, \beta, \gamma \in \mathcal{I}_\text{P} \ , \tag{21}$$

where $\Omega_\kappa \subseteq \Omega$.

Specifying $P = 1$, the entity extent measures can be decomposed for a phase as

$$\epsilon^{\overline{\overline{\alpha}}} = \sum_{i \in \mathcal{N}_\alpha} \langle 1 \rangle_{\Omega_{\alpha_i}, \Omega} = \sum_{i \in \mathcal{N}_\alpha} \epsilon^{\overline{\overline{\alpha_i}}} \quad \text{for } \alpha \in \mathcal{I}_\text{P} \ , \tag{22}$$

for an $\alpha\beta$ interface as

$$\overline{\overline{\epsilon^{\alpha\beta}}} = \sum_{i\in\mathcal{N}_\alpha} \langle 1\rangle_{\Omega_{\alpha_i\beta},\Omega} = \sum_{i\in\mathcal{N}_\alpha} \overline{\overline{\epsilon^{\alpha_i\beta}}} \quad \text{for } \alpha,\beta\in\mathcal{I}_\mathrm{P}\ , \quad (23)$$

and for the $\alpha\beta\gamma$ common curve as

$$\overline{\overline{\epsilon^{\alpha\beta\gamma}}} = \sum_{i\in\mathcal{N}_\alpha} \langle 1\rangle_{\Omega_{\alpha_i\beta,\gamma},\Omega} = \sum_{i\in\mathcal{N}_\alpha} \overline{\overline{\epsilon^{\alpha_i,\beta,\gamma}}} \quad \text{for } \alpha,\beta,\gamma\in\mathcal{I}_\mathrm{P}\ , \quad (24)$$

or

$$\overline{\overline{\epsilon^{\alpha\beta\gamma}}} = \sum_{\substack{i\in\mathcal{N}_\alpha\\ j\in\mathcal{N}_\beta}} \langle 1\rangle_{\Omega_{\alpha_i\beta_j,\gamma},\Omega} = \sum_{\substack{i\in\mathcal{N}_\alpha\\ j\in\mathcal{N}_\beta}} \overline{\overline{\epsilon^{\alpha_i,\beta_j,\gamma}}} \quad \text{for } \alpha,\beta,\gamma\in\mathcal{I}_\mathrm{P}\ . \quad (25)$$

The intrinsic macroscale fluid pressure over a region can be written as

$$p^{\alpha_i} = \langle p_\alpha\rangle_{\Omega_{\alpha_i},\Omega_{\alpha_i}} \quad \text{for } \alpha\in\mathcal{I}_\mathrm{f}\ , \quad (26)$$

and the overall macroscale fluid pressure can be written in terms of averages over regions as

$$p^\alpha = \sum_{i\in\mathcal{N}_\alpha} \langle p_\alpha\rangle_{\Omega_{\alpha_i},\Omega_\alpha} = \frac{1}{\overline{\overline{\epsilon^\alpha}}} \sum_{i\in\mathcal{N}_\alpha} \overline{\overline{\epsilon^{\alpha_i}}} p^{\alpha_i} \quad \text{for } \alpha\in\mathcal{I}_\mathrm{f}\ . \quad (27)$$

Similarly, the intrinsic macroscale capillary pressure can be obtained for an individual fluid-phase region by averaging over a subset of the interface $\Omega_{\alpha_i\beta}$, which can be formulated as

$$p^{\alpha_i\beta} = -\langle \gamma_{wn} J_w\rangle_{\Omega_{\alpha_i\beta},\Omega_{\alpha_i\beta}} \quad \text{for } \alpha,\beta\in\mathcal{I}_\mathrm{f}, \alpha\neq\beta\ , \quad (28)$$

and the macroscale capillary pressure can be recovered from the sum over all regions as

$$p^{\alpha\beta} = \frac{1}{\overline{\overline{\epsilon^{\alpha\beta}}}} \sum_{i\in\mathcal{N}_\alpha} \overline{\overline{\epsilon^{\alpha_i\beta}}} p^{\alpha_i\beta} \quad \text{for } \alpha,\beta\in\mathcal{I}_\mathrm{f}, \alpha\neq\beta\ . \quad (29)$$

Eq. (29) allows for the computation of the macroscale capillary pressure as a function of the macroscale capillary pressure of the component regions associated with a specified set of regions for either of the fluid phases. This approach is useful for the case where either of the fluid phases becomes disconnected and forms multiple connected regions, which can result for example from fingering or snap off of the non-wetting phase.

Variational methods can be used to derive a set of conditions that must hold at equilibrium in a microscale two-fluid-phase system [30]. A capillary pressure condition resulting from this analysis can be written as

$$p_{wn} + p_w - p_n + \rho_{wn}\mathbf{g}_{wn}\cdot\mathbf{n}_w = 0 \quad \text{for } \mathbf{x}\in\Omega_{wn}\ , \quad (30)$$

where $\mathbf{x}$ is a position vector that is restricted to lie on the wn interface, ρ_{wn} is the density of the wn interface, and $\mathbf{g}_{wn}$ is a body force acceleration acting on the wn interface. In the limiting case of a massless interface, Eq. (30) reduces to

$$p_{wn} + p_w - p_n = 0 \quad \text{for } \mathbf{x}\in\Omega_{wn}\ . \quad (31)$$

The macroscale equilibrium condition can be determined by applying an averaging operator to Eq. (31) yielding

$$\langle p_{wn} + p_w - p_n\rangle_{\Omega_{wn},\Omega_{wn}} = 0\ , \quad (32)$$

which can also be written as

$$\langle -\gamma_{wn} J_w + p_w - p_n\rangle_{\Omega_{wn},\Omega_{wn}} = 0\ , \quad (33)$$

or in terms of macroscale variables after evaluating the averaging operator as

$$p^{wn} + p_w^{wn} - p_n^{wn} = 0\ , \quad (34)$$

where $p^{wn} = \langle -\gamma_{wn} J_w\rangle_{\Omega_{wn},\Omega_{wn}}$, $p_w^{wn} = \langle p_w\rangle_{\Omega_{wn},\Omega_{wn}}$, and $p_n^{wn} = \langle p_n\rangle_{\Omega_{wn},\Omega_{wn}}$.

Just as the overall intrinsic macroscale average of phase pressures can be decomposed into intrinsic averages over regions, the capillary pressure can be written in terms of regional interface averages as well. Decomposition of interfacial quantities are more complicated because of the potential for the existence of multiple regions of each fluid phase. The microscale equilibrium condition given as Eq. (31) can be averaged over a region of a fluid phase yielding the regional macroscale equilibrium condition for capillary pressure given as

$$\langle p_w - p_n + p_{wn}\rangle_{\Omega_{\alpha_i\beta},\Omega_{\alpha_i\beta}} = 0 \quad \text{for } \alpha,\beta\in\mathcal{I}_\mathrm{f}, \alpha\neq\beta\ , \quad (35)$$

or evaluating the averaging operator as

$$p_w^{\alpha_i\beta} - p_n^{\alpha_i\beta} + p_{wn}^{\alpha_i\beta} = 0 \quad \text{for } \alpha,\beta\in\mathcal{I}_\mathrm{f}, \alpha\neq\beta\ , \quad (36)$$

where the subscript denotes the microscale quantity being averaged, and the superscript denotes that the averaging is computed over the fraction of the wn interface corresponding to an interaction with the closed domain of the i^{th} region of the α fluid phase.

Eq. (36) is an equilibrium condition that applies to a specified fluid region, forming an additional set of macroscale equilibrium constraints in addition to Eq. (34). However, the equilibrium conditions given by Eq. (36) will in general not agree term for term with Eq. (34). Put another way, the capillary pressure of the wn interface can vary from region to region. For example, such variation is expected for the case of disconnected regions of a non-wetting phase, which may form due to bypassing and snap-off processes and each region may then equilibrate at its own distinct rate. The resulting equilibrium capillary pressure of a region is thus affected by conditions under which the disconnected phase formed.

Note that in Eq. (34) and Eq. (36) the fluid phase pressures are averaged over a boundary of the phase. Under dynamic conditions and for irregularly shaped distributions of fluids for systems with significant gravitational

effects, these interface averaged pressures can be different from their volume averaged counterparts. When such conditions do not exist, the capillary pressure averaged over the interfacial domain $\Omega_{w_i n_j}$ can be approximated as

$$p^{w_i n_j} + p^{w_i} - p^{n_j} = 0 \, . \tag{37}$$

The volume averaged region pressures may also be good approximations for certain dynamic equations involving capillary pressure, because phase pressures equilibrate much more quickly than the interfacial curvature equilibrates [80].

Eq. (34) can be related to the set of conditions given by Eq. (37) according to

$$p^{wn} + p^{w} - p^{n} = \frac{1}{\epsilon^{\overline{\overline{wn}}}} \sum_{ij \in \mathcal{N}_{wn}} \epsilon^{\overline{\overline{w_i n_j}}} \left(p^{w_i n_j} + p^{w_i} - p^{n_j} \right) \, , \tag{38}$$

where recall that each entry in $\mathcal{N}_{wn}$ is an index pair corresponding to regions of each fluid phase, respectively. The particular weighting chosen ensures correspondence between the respective terms on each side of the equation.

In this work, we assume that the wetting phase is connected and focus on the connectivity of the non-wetting phase. In this case, Eq. (37) simplifies to an equilibrium condition for each component of the non-wetting phase:

$$p^{wn_i} + p^{w} - p^{n_i} = 0 \, . \tag{39}$$

This expression reflects that each individual component of the non-wetting phase reaches equilibrium independently of the others based on the local pore geometry. The equilibrium conditions are therefore determined independently for each individual feature. The removal of any individual non-wetting phase component does not alter the equilibria of the remaining components. It is natural to consider how changing the number of regions would affect the overall macroscale equilibrium state. Based on a particular realization of a multiphase equilibrium state, we can consider those equilibrium states that would arise if some fraction of the regions of a fluid phase were removed from the system and replaced by the region of the other fluid phase bounding the removed region. Since each non-wetting phase feature reaches it's equilibrium state independently, the removal of one feature will not effect the equilibria of the remaining features.

Given a non-wetting phase configuration that is composed of multiple components, multiple equilibrium states can be deduced based on the removal of components. That is, we may generate additional equilibrium states by considering subsets $\mathcal{C}_n \subset \mathcal{N}_n$. If some features are removed, then B_0^n will attain a new value equivalent to the cardinality of $\mathcal{C}_n$. The strategy is to manipulate directly the topology based on the equilibrium conditions and to consider the consequences for the macroscopic equilibrium relationships. Since the resulting configurations satisfy all relevant equilibrium conditions, they represent valid equilibrium states. The values of relevant macroscale quantities can be obtained from partial sums for a subset $\mathcal{C}_n$:

$$B_0^n(\mathcal{C}_n) = |\mathcal{C}_n| \, , \tag{40}$$

$$\epsilon^{\overline{\overline{n}}}(\mathcal{C}_n) = \sum_{i \in \mathcal{C}_n} \epsilon^{\overline{\overline{n_i}}} \, , \tag{41}$$

$$\epsilon^{\overline{\overline{wn}}}(\mathcal{C}_n) = \sum_{i \in \mathcal{C}_n} \epsilon^{\overline{\overline{wn_i}}} \, , \tag{42}$$

$$\epsilon^{\overline{\overline{ns}}}(\mathcal{C}_n) = \sum_{i \in \mathcal{C}_n} \epsilon^{\overline{\overline{n_i s}}} \, , \tag{43}$$

$$\chi^{\overline{\overline{n}}}(\mathcal{C}_n) = \sum_{i \in \mathcal{C}_n} \chi^{\overline{\overline{n_i}}} \, , \tag{44}$$

$$\epsilon^{\overline{\overline{wns}}}(\mathcal{C}_n) = \sum_{i \in \mathcal{C}_n} \epsilon^{\overline{\overline{wn_i s}}} \, , \tag{45}$$

$$p^{n}(\mathcal{C}_n) = \frac{1}{\epsilon^{\overline{\overline{n}}}(\mathcal{C}_n)} \sum_{i \in \mathcal{C}_n} \epsilon^{\overline{\overline{n_i}}} p^{n_i} \, , \text{ and} \tag{46}$$

$$p^{wn}(\mathcal{C}_n) = \frac{1}{\epsilon^{\overline{\overline{wn}}}(\mathcal{C}_n)} \sum_{i \in \mathcal{C}_n} \epsilon^{\overline{\overline{wn_i}}} p^{wn_i} \, . \tag{47}$$

The wetting phase properties must also be updated to reflect the removal of non-wetting phase components. The equilibrium pressure p^w remains unchanged based on the equilibrium conditions. The volume fractions and specific interfacial areas are updated as

$$\epsilon^{\overline{\overline{w}}}(\mathcal{C}_n) = \epsilon^{\overline{\overline{w}}} + \sum_{j \in \mathcal{N}_n - \mathcal{C}_n} \epsilon^{\overline{\overline{n_j}}} \, , \tag{48}$$

$$\epsilon^{\overline{\overline{ws}}}(\mathcal{C}_n) = \epsilon^{\overline{\overline{ws}}} + \sum_{j \in \mathcal{N}_n - \mathcal{C}_n} \epsilon^{\overline{\overline{n_j s}}} \, , \text{ and} \tag{49}$$

$$s^{\overline{\overline{w}}}(\mathcal{C}_n) = \frac{\epsilon^{\overline{\overline{w}}}(\mathcal{C}_n)}{\epsilon^{\overline{\overline{n}}}(\mathcal{C}_n) + \epsilon^{\overline{\overline{w}}}(\mathcal{C}_n)} \, . \tag{50}$$

III. RESULTS AND DISCUSSION

Equilibrium configurations were generated for a two-fluid-phase system within a periodic random close pack of 1,964 equally-sized spheres. The cubic computational domain was discretized to 900^3 and wetting and non-wetting phases were randomly distributed within the pore space to match a desired saturation. Equilibrium states were thereby explored by fixing the fluid saturations and allowing the fluid pressures and interfaces to relax until an equilibrium state was reached. The evolution of the multiphase system was computed at the microscale using a multiphase implementation of the lattice Boltzmann method. Full details on the implementation of the two-fluid-phase flow scheme are provided by McClure et al. [81, 82]. Further details, including a demonstration that the method is able to recover dynamic behavior of the interface and common curve from the microscale, and a resolution study for flow in porous media, are also available in the literature [83]. Once an equilibrium state was

achieved, the macroscopic state of the system was evaluated based on the results of the previous section. The connected components of the non-wetting phase were determined numerically, then averaged properties of each connected component of the non-wetting phase were then evaluated by numerically reconstructing the relevant domains to perform averaging for the phases, interfaces, and common curves [84].

Two approaches were used to initialize fluid saturations in an attempt to influence the connectivity of the non-wetting phase. For the first approach, blocks of wetting phase were randomly inserted into a domain that was initially saturated with a fully-connected non-wetting phase. The second approach considered the insertion of blocks of non-wetting phase into a system initially saturated with wetting phase. We find that either initialization procedure can be used to generate two-fluid configurations as needed to capture the relationships explored in this work. In both cases cubic blocks of phase were added to the system until a specified wetting phase saturation was achieved. The three dimensional position of the inserted blocks was determined randomly. The size of the individual blocks was 32^3. Any portion of an inserted block that overlapped with the solid phase remained as solid phase. Note that no attempt was made to generate physically probable initial configurations for the phase locations; we simply sought to explore a wide range of possible equilibrium states. Thus, the objective was to sample the space of possible microscale states and evaluate the corresponding macroscale state.

Based on the initial phase configurations, a range of different microscale equilibrium states were reached. The connectivity of a phase determines the energetic states that are possible. Molecules within a particular component of the non-wetting phase can only explore the energetic states that are accessible locally, which is constrained by the topology. To account for this, it is natural to consider the Euler characteristic as a way to quantitatively account for the role of topology at the macroscale, since it is the relevant topological invariant that accounts for the connectivity of an object. Due to the discrete width of the interfacial region in the LBM, a fully connected wetting phase is obtained for each of the cases considered.

The set of simulations performed included 46 equilibrium configurations distributed across $0 < s^{\overline{\overline{w}}} < 1$. We consider possible states by generating a sequence of subsets for each realization. Given a particular multiphase configuration, the non-wetting phase components were indexed based on their volume fraction such that $\epsilon^{\overline{\overline{n_1}}} > \epsilon^{\overline{\overline{n_2}}} > \ldots > \epsilon^{\overline{\overline{n_{N_c}}}}$. We then defined a sequence of subsets $\mathcal{C}_n^{(k)}$, such that all non-wetting components $i \leq k$ are included in $\mathcal{C}_n^{(k)}$. Non-wetting components with $i > k$ were removed from the system. Macroscopic states were evaluated by applying Eqs. (41) – (50) based on $\mathcal{C}_n^{(k)}$ for $k = 1, 2, \ldots, B_0^n$. This approach allowed equilibrium states to be generated in a very computationally efficient manner. Since fluid saturations were initialized randomly, arbitrarily many configurations could be simulated in parallel. Furthermore, when the non-wetting phase was comprised of multiple connected components, additional macroscopic states could be generated based on the results of the previous section. Applying this approach yielded a total of 42,908 macroscopic states from the set of 46 initial fluid configurations. The resulting dense set of equilibrium points was used to evaluate the uniqueness of the relationships $p^{wn}(s^{\overline{\overline{w}}})$, $p^{wn}(s^{\overline{\overline{w}}}, \epsilon^{\overline{\overline{wn}}})$, and $p^{wn}(s^{\overline{\overline{w}}}, \epsilon^{\overline{\overline{wn}}}, \chi^{\overline{\overline{n}}})$.

The equilibrium relationship between the macroscale capillary pressure, fluid saturation, specific interfacial area, the Euler characteristic, and the specific common curve length as a function of B_0^n is explored in Fig. 2. Quantities are plotted in non-dimensional form based on the sphere diameter $D = 83.67\ \delta x$ and interfacial tension $\gamma^{wn} = 30$ mN/m, where the lattice length was $\delta x = 1.0\ \mu$m. To obtain an equilibrium configuration using the lattice Boltzmann method, 1.8×10^6 time steps were required. The simulation was continued until the macroscopic value of the interfacial curvature stabilized. Based on the results of previous study, the timescale required for the curvature to reach an equilibrium state is longer than the time required for other macroscopic variables of interest to equilibrate, in particular the fluid pressures [80]. The error associated with the curvature measurement was estimated by computing $\varepsilon_J = |p_w^{wn} - p_n^{wn} - \gamma^{wn} J_w^{wn}|$, a quantity that is identically zero at equilibrium. This error is plotted in Fig. 3 Deviations from zero are considered to be numerical errors associated with the measurement of the interfacial curvature. The mean error is 1.58% over all configurations. Significantly larger errors are encountered when the interfacial curvatures are high. These errors are most apparent at very low wetting phase saturations. As the curvature increases, the radius of curvature decreases. For example, when $p^{wn} = 10$ the mean radius of curvature is 13.3 δx, $p^{wn} = 20$, the mean radius of curvature is only 6.67 δx. The interfacial width in the LBM is $\sim 3\ \delta x$, so a decrease in accuracy is inevitable at high curvatures. When the capillary pressure is high, measurements of the interfacial curvature will tend to underestimate the true value as a result.

The value of p^{wn} is plotted as a function of fluid saturation in Fig. 2(a). This relationship demonstrates similar features as compared to experimentally determined relationships. Nevertheless, it is important to distinguish the capillary pressure-saturation data plotted in Fig. 2(a) and the capillary pressure-saturation data generated from standard experiments. In experiments the capillary pressure is typically determined from the difference between the phase pressures measured at the boundary of the system. At equilibrium, this will match the capillary pressure of the non-wetting component that is connected to the boundary. The capillary pressure of trapped non-wetting is not taken into consideration. However, the volume of these features do

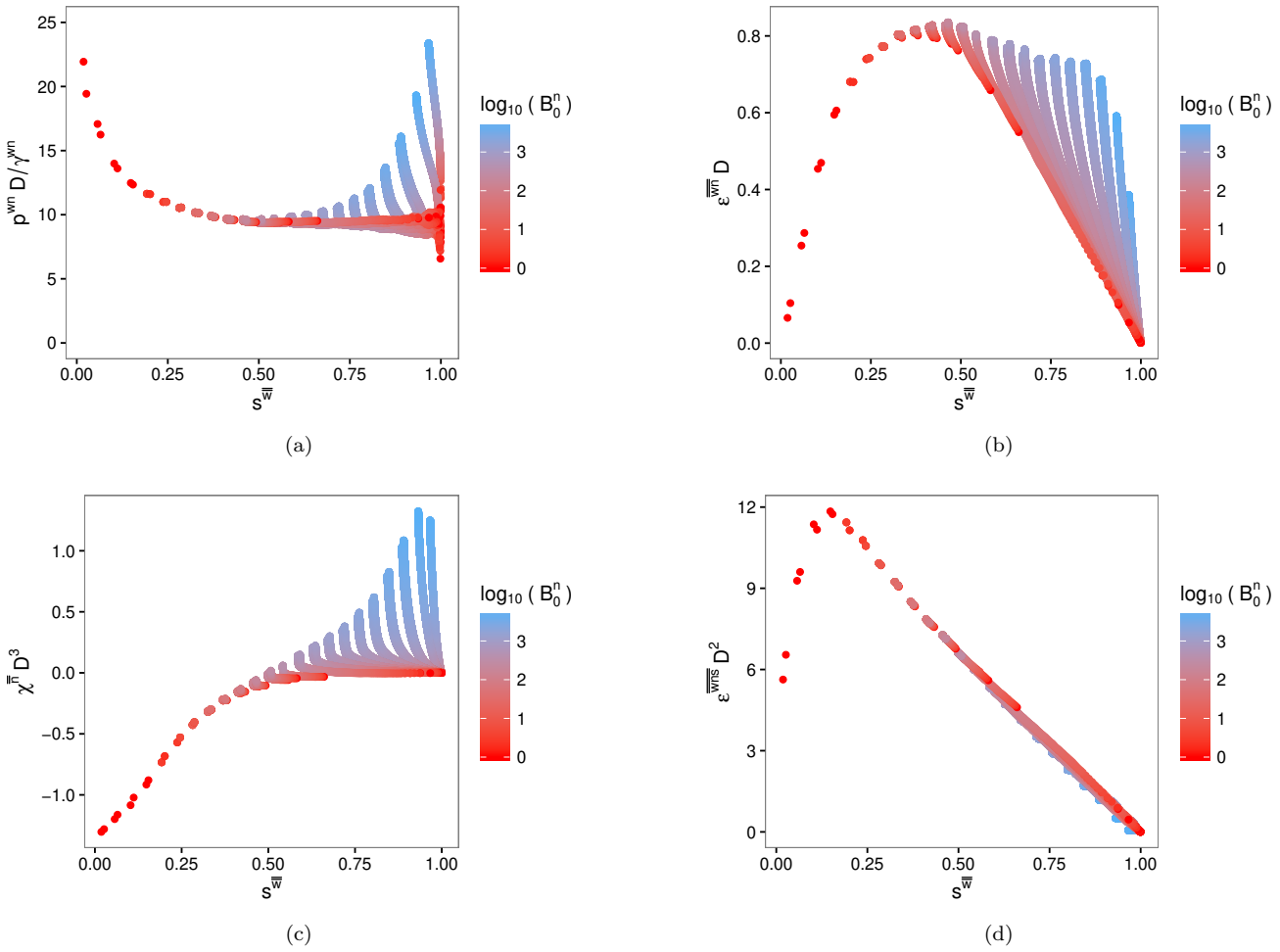

FIG. 2. Equilibrium quantities plotted in non-dimensional form as a function of the wetting phase saturation $s^{\overline{\overline{w}}}$ and the number of features B_0^n: (a) capillary pressure; (b) specific interfacial area per unit volume; (c) Euler characteristic per unit volume; and (d) specific common curve length per unit volume.

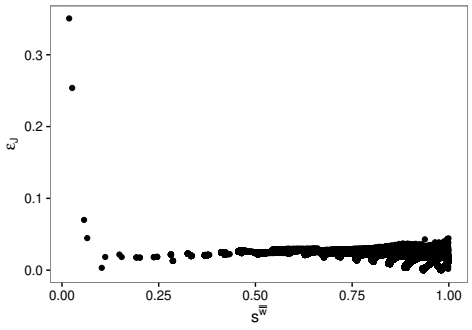

FIG. 3. Relative error for the interfacial curvature for equilibrium configurations generated from the lattice Boltzmann method. The mean error is 1.5 %; significantly higher errors are encountered when the interfacial curvature is large.

contribute to measured values of saturation, since these are also determined from the boundary—if the results are not represented in terms of a transformed saturation. Thus, the two variables may be measured in a fundamentally inconsistent way. In Fig. 2(a), the capillary pressure is determined as an average over the entire interface Ω_{wn}, weighting each feature according to the amount of interface—it is simply the average capillary pressure of the system.

The specific interfacial area per unit volume and specific length of the common curve per unit volume are plotted in non-dimensional form in Fig. 2(b) and Fig. 2(d), respectively. While the length of the common curve can be reasonably approximated as a function of the fluid saturation, the specific interfacial area can take on multiple values for a given value of $s^{\overline{\overline{w}}} > 0.25$. The possible values are clearly associated with the number of non-wetting phase components in the system, with the minimum interfacial area corresponding to a small number of features. This is the case because a larger and more well connected non-wetting phase has the tendency to minimize the global surface energy. This global mini-

mum is inaccessible from fluid configurations with a large number non-wetting phase components.

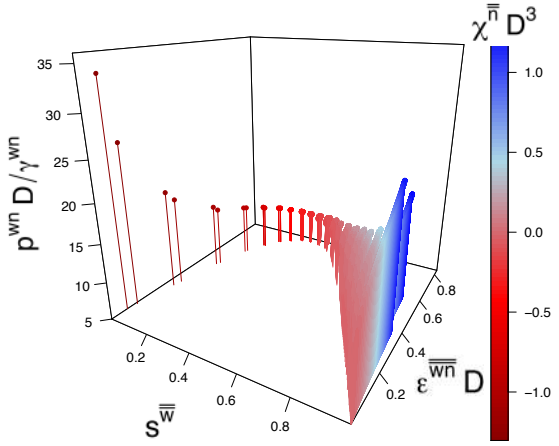

FIG. 4. Data points for the relationship between the fluid saturation, specific interfacial area, capillary pressure, and Euler characteristic.

Previous studies have focused primarily on the development of empirical functional forms to predict the capillary pressure. Among these forms are traditional relationships between the capillary pressure and fluid saturation, $p^{wn}(s^{\overline{\overline{w}}})$, such as those defined by Leverett, [85], van Genuchten [86], and Brooks and Corey [87]. More recently, efforts have focused on studying the role of interfacial area as an additional state variable. [48, 88–92]. While neither p^{wn} nor $\epsilon^{\overline{\overline{wn}}}$ are a unique function of the fluid saturation, it has been suggested that $p^{wn}(s^{\overline{\overline{w}}}, \epsilon^{\overline{\overline{wn}}})$ is a unique function. In this context, the data plotted in Fig. 2(a) and Fig. 2(b) result from the projection of a three-dimensional system onto a two-dimensional plane. Many authors have continued the tradition of empirically constructing analytic functional forms to approximate trends observed from data [45, 49, 93–97]. In this work, we consider a very dense set of points that can be used to quantitatively evaluate the uniqueness of the relationship between capillary pressure and other geometric variables. The set of data points generated are shown in Fig. 4, with the Euler characteristic plotted in color. The surface shows that the possible values for the interfacial area are constrained to a ribbon, with the width of this ribbon increasing when a relatively large number of non-wetting phase components are possible. For low wetting phase saturations where the non-wetting phase is almost entirely connected, the interfacial area tends to take on only a single value for a given fluid saturation. For $s^{\overline{\overline{w}}} > 0.5$, many possible configurations are possible due to the fact that the non-wetting phase is divided into a large number of components that occupy different parts of the pore space. Since the connectedness of the non-wetting phase is directly related to $\chi^{\overline{\overline{n}}}$, the Euler characteristic is likely to be important to characterize the average behavior of these microstates.

An important aspect of the analysis of the data presented in Fig. 4 is the method used to assess the uniqueness of multi-dimensional relationships. If we consider $p^{wn}(s^{\overline{\overline{w}}})$, $p^{wn}(s^{\overline{\overline{w}}}, \epsilon^{\overline{\overline{wn}}})$, and $p^{wn}(s^{\overline{\overline{w}}}, \epsilon^{\overline{\overline{wn}}}, \chi^{\overline{\overline{n}}})$ as a hierarchy of macroscopic approximations designed to capture the essential information from the microscopic states, we must then develop a consistent approach to assess how well these various approximations perform. While the data should be smooth if a unique function exists, constraining the fits to a posited specific particular functional form introduces additional errors that can be avoided if more general relationships are considered. In order to assess the impact of additional variables, errors must be assessed in a consistent way for higher dimensional data sets. Generalized additive models (GAMs) provide a straightforward means to address the challenges of evaluating smooth relationships for multi-dimensional data sets, and estimating the associated errors. GAMs are routinely applied to produce locally-smooth spline approximations for general data. We rely on the GAM implementation available in the `mgcv` package within the R software distribution. A complete description of the procedure used to produce the GAM fits for this paper is provided by Wood et al. [98–100]. A predictor is constructed from a sum of smooth basis functions, with coefficients that are automatically determined from the data based on principles of maximum likelihood. Fits are determined using generalized cross-validation (GCV) with tensor product smoothing penalties to ensure the surface is smooth. The ability of the GAM to explain the variance within the data indicates the extent to which the functional form explains the observed behavior. We generated GAM fits for each of the relationships $p^{wn}(s^{\overline{\overline{w}}})$, $p^{wn}(s^{\overline{\overline{w}}}, \epsilon^{\overline{\overline{wn}}})$, and $p^{wn}(s^{\overline{\overline{w}}}, \epsilon^{\overline{\overline{wn}}}, \chi^{\overline{\overline{n}}})$. The residuals for the fits are plotted in Fig. 5. Results clearly demonstrate that successively better approximations are obtained when including the interfacial area and the Euler characteristic. The implication is that including a measure of connectivity is important to characterize systems where many topologically distinct microstates are possible. The Euler characteristic is especially important at high wetting phase saturations, due to the fact that as the non-wetting phase becomes increasingly disconnected many configurations are possible. All three relationships are non-unique in the immediate vicinity of $s^{\overline{\overline{w}}} = 1$. This is unsurprising, since as $s^{\overline{\overline{w}}} \to 1$, $awn \to 0$ but p^{wn} is undefined in the limit. For the low non-wetting phase saturation limit, the non-wetting fluid is trapped in a small number of components. Depending on the pores where these components are trapped, a different p^{wn} will be obtained, and the relationships become non-unique.

The mean and median absolute relative errors were computed based on the information plotted in Fig. 5. These values were 15%, and 8%, $p^{wn}(s^{\overline{\overline{w}}})$ 1%, 0.8% for $p^{wn}(s^{\overline{\overline{w}}}, \epsilon^{\overline{\overline{wn}}})$, and 0.3%, 0.2% for $p^{wn}(s^{\overline{\overline{w}}}, \epsilon^{\overline{\overline{wn}}}, \chi^{\overline{\overline{n}}})$. From

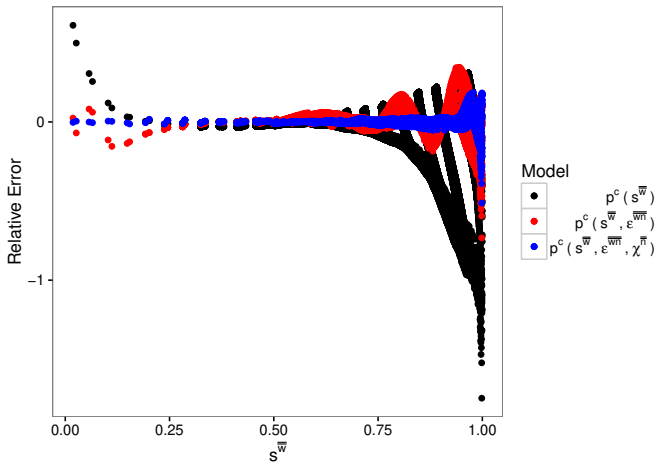

FIG. 5. Residual for GAM fits associated with each of the relationships $p^{wn}(s^{\overline{w}})$, $p^{wn}(s^{\overline{w}}, \epsilon^{\overline{wn}})$ and $p^{wn}(s^{\overline{w}}, \epsilon^{\overline{wn}}, \chi^{\overline{n}})$. Including the interfacial area reduces the hysteresis significantly, and including both the interfacial area and Euler characteristic eliminates nearly all hysteresis from the underlying data.

these results, it is clear that including the interfacial area does not completely eliminate hysteresis observed in the $p^{wn}(s^{\overline{w}})$ relationship. This is attributed to the fact that connectivity is an essential aspect of the topology of a phase, which constrains the equilibrium states that are accessible to the system. The Euler characteristic provides a quantitative measure of the connectivity such that the microscale states can be characterized more completely at the macroscale.

IV. SUMMARY AND CONCLUSIONS

- Theory was developed to describe interfacial equilibrium conditions for a multiphase porous medium system in which the non-wetting phase is subdivided into an arbitrary number of connected components.
- An efficient approach was developed to generate equilibrium states based on the connected non-wetting phase components and used to evaluate directly the corresponding equilibrium states at the macroscale.
- A dense set of 42,908 equilibrium configurations were generated to determine equilibrium values for the fluid saturation, phase pressures, interfacial curvatures, specific interfacial areas, and specific length of the common curve.
- Analysis of the equilibrium data demonstrates that a relationship among capillary pressure, interfacial area, and Euler characteristic removes nearly all of the hysteresis in the capillary pressure relationship.

ACKNOWLEDGEMENTS

This work was supported by Army Research Office grant W911NF-14-1-02877, Department of Energy grant DE-SC0002163, and National Science Foundation grant 1619767. An award of computer time was provided by the Department of Energy INCITE program. This research also used resources of the Oak Ridge Leadership Computing Facility, which is a DOE Office of Science User Facility supported under Contract DE-AC05-00OR22725.

[1] E. Saadatpoor, S.L. Bryant, and K. Sepehrnoori, Transp. Porous Media, **82**, 3 (2010).
[2] J.C.M. Pires, F.G. Martins, M.C.M. Alvim-Ferraz, and M.Simoes, Chem. Eng. Res. & Design, **89**,1446 (2011).
[3] M.D. Zoback and S.M. Gorelick, PNAS, **109**, 10164 (2012).
[4] M.G. Gerritsen and L.J. Durlofsky, Annual Rev. Fluid Mech., **37**, 211 (2005).
[5] N. Djilali, Energy, **32**, 269 (2007).
[6] V. Gurau and J.A. Mann, SIAM J on Applied Mathematics, **70**, (2009).
[7] J. Zhang, Microfluidics and Nanofluidics, **10**, 1 (2011).
[8] R. Anderson, L. Zhang, Y. Ding, M. Blanco, X. Bi, and D.P. Wilkinson, J. of Power Sources, **195** 4531 (2010).
[9] R. Hilfer, R.T. Armstrong, S. Berg, A. Georgiadis, and H. Ott, Phys. Rev. E, **92**, 063023 (2015).
[10] H.S. Wiklund and T. Uesaka, Phys. Rev. Rev. E, **87**, 023006 (2013).
[11] C. Cottin, H. Bodiguel, and A. Colin, Phys. Rev. E, **84**, 026311 (2011).
[12] K.T. Tallakstad, G. Lovoll, H.A. Knudsen, T. Ramstad, E.G. Flekkoy, and K.J. Maloy, Phys. Rev. E, **80**, 036308 (2009).
[13] K.T. Tallakstad, H.A. Knudsen, T. Ramstad, G. Lovoll, K.J. Maloy, R. Toussaint, and E.G. Flekkoy, Phys. Rev. Letters, **102**, 074502 (2009).
[14] L. Cueto-Felgueroso and R. Juanes, Phys. Rev. Letters, **101**, 244504 (2008).
[15] C.U. Hatiboglu and T. Babadagli, Phys. Rev. E, **77**, 066311(2008).
[16] M. Ferer, G.S. Bromhal, and D.H. Smith, Phys. Rev. E, **71**, 026303 (2005).
[17] L. Zhou, Z.G. Qu, T. Ding, and J.Y. Miao, Phys. Rev. E, **93**, 043101 (2016).
[18] Y. Hu, D. Li, S. Shu, and X. Niu, Phys. Rev. E, **93**, 023308 (2016).

[19] L. Chen, Q. Kang, B.A. Robinson, Y. He, and W. Tao, Phys. Rev. E, **87**, 043306 (2013).

[20] D. Reeves and D.H. Rothman, Phys. Rev. E, **86**, 031120 (2012).

[21] M. Piri and M.J. Blunt, Phys. Rev. E, **71** 26301 (2005).

[22] M.S. Al-Gharbi and M.J. Blunt, Phys. Rev. E, **71**, 016308 (2005).

[23] M.G. Rozman and M. Utz, Phys. Rev. Letters, **89**, 135501 (2002).

[24] M.C. Sukop, H. Huang, C.L. Lin, M.D. Deo, K.Oh, and J.D. Miller. Phys. Rev. E, **77**, 026710 (2008).

[25] M. Piri and Z.T. Karpyn, Phys. Rev. E, **76**,016316 (2007).

[26] R. Holtzman and E. Segre, Phys. Rev. Letters, **115**, 164501 (2015).

[27] P.K. Mondal, D. DasGupta, and S. Chakraborty, Phys. Rev. E, **90**, 013003 (2014).

[28] R.T. Armstrong and S. Berg, Phys. Rev. E, **88** , 043010 (2013).

[29] Z.T. Karpyn and M. Piri, Phys. Rev. E, **76**, 016315 (2007).

[30] W.G. Gray and C.T. Miller, Introduction to the Thermodynamically Constrained Averaging Theory for Porous Medium Systems. (Springer, Zürich, 2014).

[31] B. Amaziane, J.P. Milisic, M. Panfilov, and L. Pankratov, Phys. Rev. E, **85**, 016304 (2012).

[32] R. Hilfer, Phys. Rev. E, **73**, 016307 (2006).

[33] S.M. Hassanizadeh and W.G. Gray, Adv. Water Res., **16**, 53 (1993).

[34] R.I. Al-Raoush and C.S. Wilson, J. Hydrol., **300**, 44 (2005).

[35] C.J. Landry, Z.T. Karpyn, and M. Piri, Geofluids, **11**, 209 (2011).

[36] M.L. Porter, D. Wildenschild, G. Grant, and J.I. Gerhard, Water Resour. Res., **46** W08512 (2010).

[37] M.L. Porter and D. Wildenschild, Comp. Geosci., **14**, 15 (2010).

[38] S. Peng and M.L. Brusseau, J. of Hydrol. Eng., **17** 829 (2012).

[39] M.J. Blunt, B. Bijeljic, H. Dong, O. Gharbi, S. Iglauer, P. Mostaghimi, A. Paluszny, and C. Pentland, Adv. Water Res., **51**, 197, (2013).

[40] D. Wildenschild and A.P. Sheppard, Adv. Water Res., **51**, 217, (2013).

[41] S. Berg, H. Ott, S.A. Klapp, A. Schwing, R. Neiteler, N. Brussee, A. Makurat, L. Leu, F. Enzmann, J. Schwarz, M. Kersten, S. Irvine, and M. Stampanoni. PNAS, **110**, 3755, (2013).

[42] A.L. Herring, E.J. Harper, L. Andersson, A. Sheppard, B.K. Bay, and D. Wildenschild, Adv. Water Res., **62**, 47, (2013).

[43] C. Pan, M. Hilpert, and C.T. Miller, Water Resour. Res., **40**, W01501 (2004).

[44] M.G. Schaap, M.L. Porter, B.S.B. Christensen, and D.Wildenschild, Water Resour. Res., **43**, W12S06 (2007).

[45] M.L. Porter, M.G. Schaap, and D.Wildenschild, Adv. Water Res., **32**,1632 (2009).

[46] E. Jettestuen, J.O. Helland, and M. Prodanovic, Water Resour. Res., **49**, 4645 (2013).

[47] A. Georgiadis, S. Berg, A. Makurat, G. Maitland, and H. Ott, Phys. Rev. E, **88**, 033002 (2013).

[48] J.T. Cheng, L.J. Pyrak-Nolte, D.D. Nolte, and N.J. Giordano. Geophys. Res. Lett. **31**, L08502 (2004).

[49] V. Joekar-Niasar and S.M. Hassanizadeh, Water Resour. Res., **47**, W05513 (2011).

[50] V. Joekar-Niasar and S.M. Hassanizadeh, Transp. Porous Meda, **94**, 465 (2012).

[51] I. Chatzis, N.R. Morrow, and H.T. Lim, SPE Journal, **24**, 311 (1983).

[52] I.Chatzis, M.S. Kuntamukkula, and N.R. Morrow, SPE Reservoir Eng., **3**, 902 (1988).

[53] N.R. Morrow, I.Chatzis, and J.J. Taber, SPE Reservoir Eng., **2**, 927 (1988).

[54] S.H. Conrad, J.L. Wilson, W.R. Mason, and W.J. Peplinski, Water Resour. Res., **28**, 467 (1992).

[55] A.S. Mayer and C.T. Miller, J. of Contaminant Hydrology, **11**, 189 (1992).

[56] M. Hilpert, J.F. McBride, and C.T. Miller, Adv. Water Res., **24**, 157 (2000).

[57] M.I. Lowry and C.T. Miller, Water Resour. Res., **31**, 455 (1995).

[58] V. Joekar-Niasar, F. Doster, R.T. Armstrong, D. Wildenschild, and M.A. Celia, Water Resour. Res., **49**, 4244 (2013).

[59] T. Chevalier, D. Salin, L. Talon, and A.G. Yiotis, Phys. Rev. E, **91**, 043015 (2015).

[60] T. Ramstad and A. Hansen, Phys. Rev. E, **73**, 026306 (2006).

[61] S. Schlüter, S. Berg, M. Rücker, R.T. Armstrong, H.-J. Vogel, R. Hilfer, and D. Wildenschild, Water Resour. Res.,**52**, 2194 (2016).

[62] E. Shahraeeni and D. Or, Phys. Rev. E, **85**, 016317 (2012).

[63] M.R. Deinert and J-Y. Parlange, Phys. Rev. E, **79**, 021202 (2009).

[64] L. Xu, S. Davies, A.B. Schofield, and D.A. Weitz, Phys. Rev. Letters, **101**, 094502 (2008).

[65] P. Lehmann, S. Assouline, and D. Or, Phys. Rev. E, **77**, 056309 (2008).

[66] J. Bear and A.H.D. Cheng, In Modeling Groundwater Flow and Contaminant Transport, volume23 of Theory and Applications of Transport in Porous Media, (2010).

[67] J. Bear, B. Rubinstein, and L. Fel, Transp. Porous Media, **89**, (2011).

[68] D.C. Standnes and T. Austad, Colloids and Surfaces A-Physiochemical and Eng. Aspects, **216**, 243 (2003).

[69] G. Harrold, D.C. Gooddy, D.N. Lerner, and S.A. Leharne, Env. Sci. & Tech., **35**, 1504 (2001).

[70] K.R. Mecke, International J. of Modern Physics B, **12**, 861 (1998).

[71] C.H. Arns, M.A. Knackstedt, and K.R. Mecke, Colloids and Surfaces-Physiochemical and Eng. Aspects, **241**, 351 (2004).

[72] C.H. Arns, M.A. Knackstedt, and K. Mecke, J. of Microscopy, **240**, 181 (2010).

[73] H.J. Vogel, U. Weller, and S. Schlueter, Comp. & Geosci., **36**, 1236 (2010).

[74] R. Hilfer, Transp. Porous Media, **46**, 373 (2002).

[75] P. Lehmann, P. Wyss, A. Flisch, E. Lehmann, P. Vontobel, M. Krafczyk, A. Kaestner, F. Beckmann, A. Gygi, and H. Fluhler, Vadose Zone J., **5**, 80 (2006).

[76] P. Lehmann, M. Berchtold, B. Ahrenholz, J. Toelke, A. Kaestner, M. Krafczyk, H. Fluhler, and H.R. Kunsch, Adv. Water Res., **31**, 1188 (2008).

[77] S. Schlueter and H.-J. Vogel, Adv. Water Res., **34**, 314 (2011).

[78] H.J. Vogel, In Mecke, K. and Stoyan, D., editor, Morphology of Condensed Matter: Physics and Geometry of Spatially Complex Systems, volume 600 of Lecture Notes in Physics, (2002).
[79] A. Huang, H. Liu, C. Lee, C. Yang, and Y. Tsang, IEEE Trans. on Medical Imaging, **28**, 43 (2009).
[80] W.G. Gray, A.L. Dye, J.E. McClure, L.J. Pyrak-Nolte, and C.T. Miller, Water Resour. Res., **51**, 5365 (2015).
[81] J.E. McClure, J.F. Prins, and C.T. Miller, Comp. Phys. Comm., **185**, 1865 (2014).
[82] J.E. McClure, H. Wang, J.F. Prins, C.T. Miller, and W. Feng, Petascale application of a coupled CPU-GPU algorithm for simulation and analysis of multiphase flow solutions in porous medium systems. In 28th IEEE International Parallel& Distributed Processing Symposium, Phoenix, Arizona, (2014).
[83] J.E. McClure, M.A.Berrill, W.G.Gray, and C.T.Miller, J. of Fluid Mech., **796**, 211 (2016).
[84] J.E. McClure, D. Adalsteinsson, C. Pan, W.G. Gray, and C.T. Miller, Adv. Water Res., **30**, 354 (2007).
[85] M.C. Leverett, Petroleum Transactions, AIME, **142**, 152 (1941).
[86] M.T. van Genuchten, Soil Science Society of America J., **44**, 892 (1980).
[87] R.H. Brooks and A.T. Corey, J. of the Irrigation and Drainage Division, Proceedings of the American Society of Civil Engineers, **61** (1966).
[88] P.C. Reeves and M.A. Celia, Water Resour. Res., **32**, 2345 (1996).
[89] R.J. Held and M.A. Celia, Adv. Water Res., **24** 325 (2001).
[90] R.J. Held and M.A. Celia, Water Resour. Res., **37** 165 (2001).
[91] K.A. Culligan, D. Wildenschild, B.S.B. Christensen, W.G. Gray, M.L. Rivers, and A.F.B. Tompson, Water Resour. Res., **40**, W12413 (2004).
[92] K.A. Culligan, D. Wildenschild, B.S.B. Christensen, W.G. Gray, and M.L. Rivers, Adv. Water Res., **29**, 227 (2006).
[93] M.L. Brusseau, S. Peng, G. Schnaar, and M.S. Costanza-Robinson, Water Resour. Res., **42**, W03501 (2006).
[94] M.L. Brusseau, S. Peng, G. Schnaar, and A. Murao, Env. Sci. & Tech., **41**, 1956 (2007).
[95] S. Peng and M.L. Brusseau, J. of Hydrol. Eng., **17**, 829 (2012).
[96] V. Joekar-Niasar, S. Hassanizadeh, and A. Leijnse, Transp. Porous Media, **74**, 201 (2008).
[97] V. Joekar-Niasar, M. Prodanović, D. Wildenschild, and S.M. Hassanizadeh, Water Resour. Res., **46**, W06526 (2010).
[98] S.N. Wood, J. Royal Stat. Soc. Ser. B-Stat. Meth., **70**, 495 (2008).
[99] S.N. Wood, F. Scheipl, and J.J. Faraway, Stat. Comp., **23**, 341(2013).
[100] S.N. Wood, Y. Goude, and S. Shaw, J. Royal Stat. Soc. Ser. C-Applied Stat., **64**, 139, (2015).